Electronic Supplementary Information

Rationally constructing hierarchical two-dimensional NiCo metal–organic framework/graphene hybrid for highly efficient Li+ ions storage

Jun Jin,[a, c] You-fang Zhang,[b,*] Huanwen Wang,[a] Yansheng Gong,[a] Rui Wang,[a] Beibei He,[a] Tuo Xiao,[a] Yun Zheng,[d] Xianhu Liu,[e] and Kun Zhou[c,f,*]

[a]Faculty of Materials Science and Chemistry, China University of Geosciences, Wuhan 430074, China.

[b]Hubei Key Laboratory of Polymer Materials, School of Materials Science and Engineering, Hubei University, Wuhan 430062, China. Email: 20190149@hubu.edu.cn

[c]School of Mechanical and Aerospace Engineering, Nanyang Technological University, 50 Nanyang Avenue, Singapore 639798, Singapore. Email: kzhou@ntu.edu.sg

[d]Key laboratory of optoelectronic Chemical Materials and Devices, Ministry of Education, Jianghan University, Wuhan 430056, China.

[e]National Engineering Research Center for Advanced Polymer Processing Technology, Zhengzhou University, Zhengzhou 450002, China.

[f]Environmental Process Modeling Center, Nanyang Environment and Water Research Institute, Singapore 637141, Singapore.

Experimental

Characterizations

The morphology and structures of the samples were characterized by scanning electron microscopy (SEM, JEOL, JSM-7600F) and field emission transmission electron microscopy (TEM, JEOL, JEM-2100F) operating at 200 kV. The X-ray diffraction (XRD) measurement was performed on a Shimadzu XRD-600 instrument with Cu Kα radiation (λ = 0.15404 nm) operating at 40 kV and 30 mA. The Raman spectra are obtained using a 514 nm micro-Raman spectrometer (Renishaw). The nitrogen adsorption-desorption isotherms and Brunauer–Emmett–Teller (BET) surface areas were measured using a Micrometrics equipment (Tri-star II 3020). The X-ray photoelectron spectroscopy (XPS) characterizations were conducted on a Theta Probe electron spectrometer (VG ESCALAB200i-XL, Thermal Scientific).
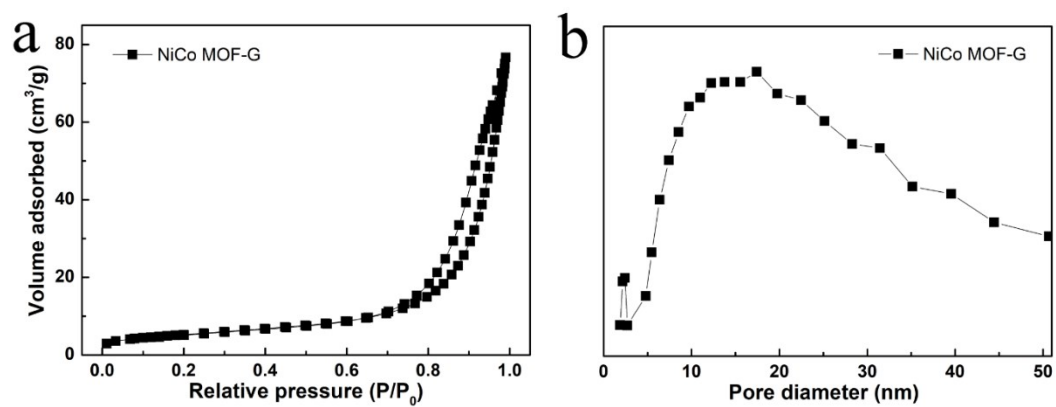
Electrochemical measurements

The electrochemical performances of the 2D MOF-G hybrid electrodes were evaluated in 2032-type coin cells, which were assembled in an argon-filled glove box (MBraun, Inc.) with the concentrations of moisture and oxygen below 0.1 ppm. Lithium metal was used as the counter/reference electrode and 1 M $LiPF_6$ in ethylene carbonate (EC)/dimethyl carbonate (DMC) was used as the electrolyte. The working electrode slurries were prepared by mixing the active material (*e.g.*, NiCo MOF-G), carbon black (Super P), and polyvinylidene fluoride (PVDF) in a mass ratio of 8:1:1. The homogeneous slurry was then uniformly coated on a copper foil (12 mm in diameter) and dried at 60 °C under vacuum for 12 h. The loading density of active materials (*e.g.*, NiCo MOF-G) in the electrodes is ~1.2 mg cm^{-2}. Galvanostatic

discharge/charge tests were performed on a Neware battery tester between 0.02 and 3.0 V *versus* Li/Li$^+$. Cyclic voltammetry (CV, 0.02–3.0 V) tests were conducted on a Solartron electrochemical workstation. The electrochemical impedance spectroscopy (EIS, 1 MHz–0.1 Hz) spectra were measured using a Zennium Pro electrochemical workstation. The potentiodynamic EIS (PEIS) spectra were collected on the Zennium Pro workstation while the battery unit was discharged/charged at a current density of 1 A g^{-1}.

Results and discussion

Table S1. Comparison of the electrochemical properties of MOF-based anode materials.

| Anode material	Capacity / mAh g^{-1} (cycle number)	Current density / A g^{-1}	Ref.
Mn MOF	607 (400)	0.5	[1]
Mn MOF	390 (50)	0.05	[2]
Cu MOF	474 (50)	0.383	[3]
Mn MOF	494 (500)	1	[4]
Al MOF	392 (100)	0.0375	[5]
Fe MOF/rGO	550 (100)	0.1	[6]
Co MOF/rGO	639 (120)	0.5	[7]
Zn MOF	480 (10)	0.5	[8]
Co MOF	358 (200)	0.1	[9]
Co MOF	435 (1000)	1	[10]
Cd MOF	~380 (10)	1	[11]
Fe MOF	75 (50)	0.002	[12]
NiCo MOF-G	920 (10) 736 (10) 640 (500) 424 (500)	0.1 0.5 1 3	This work

Figure S1. (a) N_2 adsorption-desorption isotherm and (b) pore size distribution of the NiCo MOF-G hybrid. The BET specific surface area (S_{BET}) of the NiCo MOF-G hybrid is 19 m^2 g^{-1}.
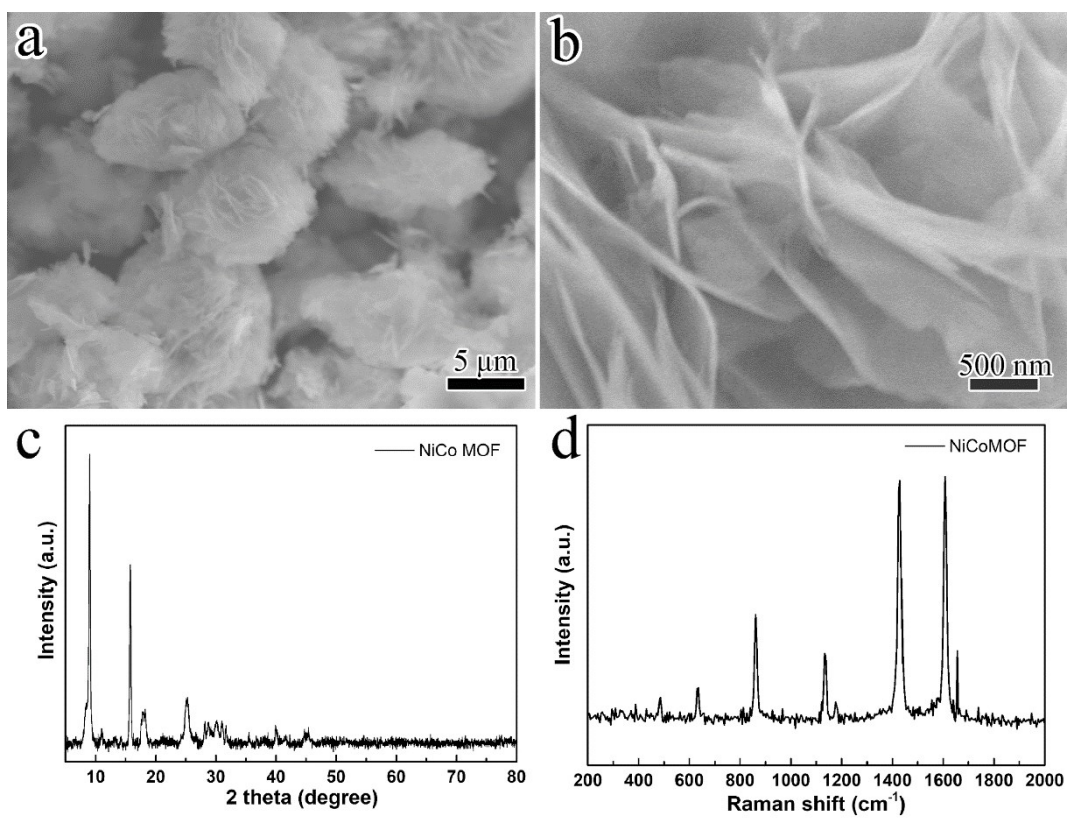
Figure S2. (a, b) SEM images, (c) XRD pattern, and (d) Raman spectrum of the 2D NiCo MOF

sample.
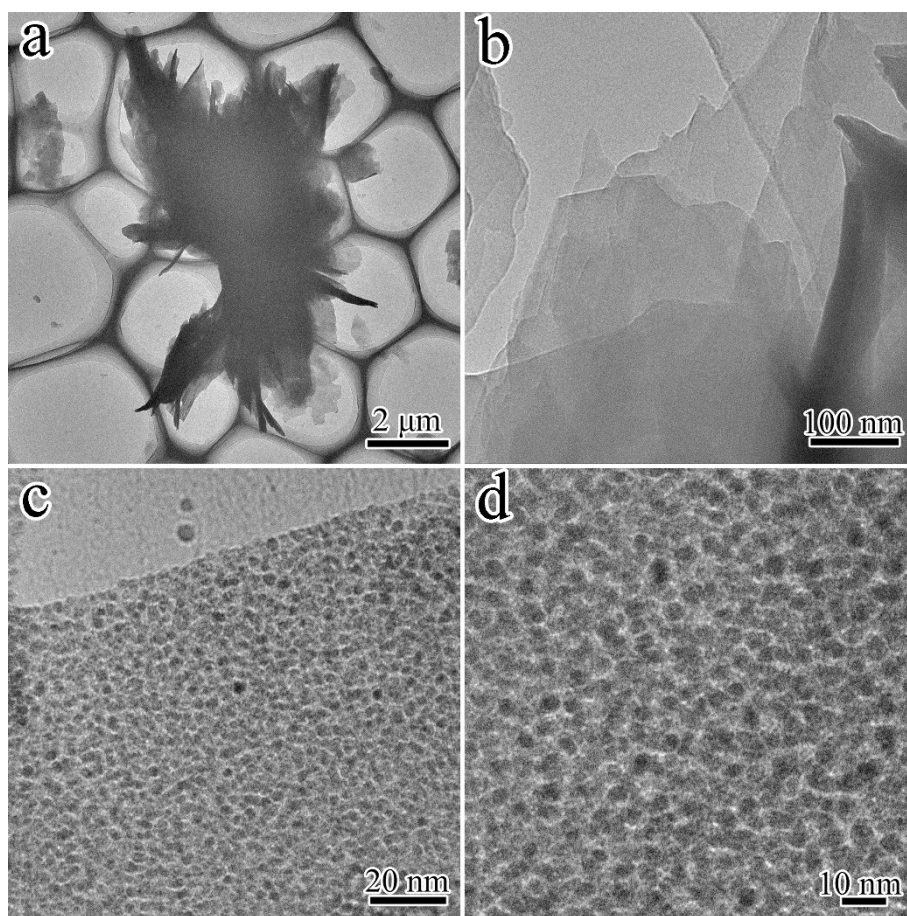
**Figure S3.** (a–d) TEM images of the 2D NiCo MOF sample.
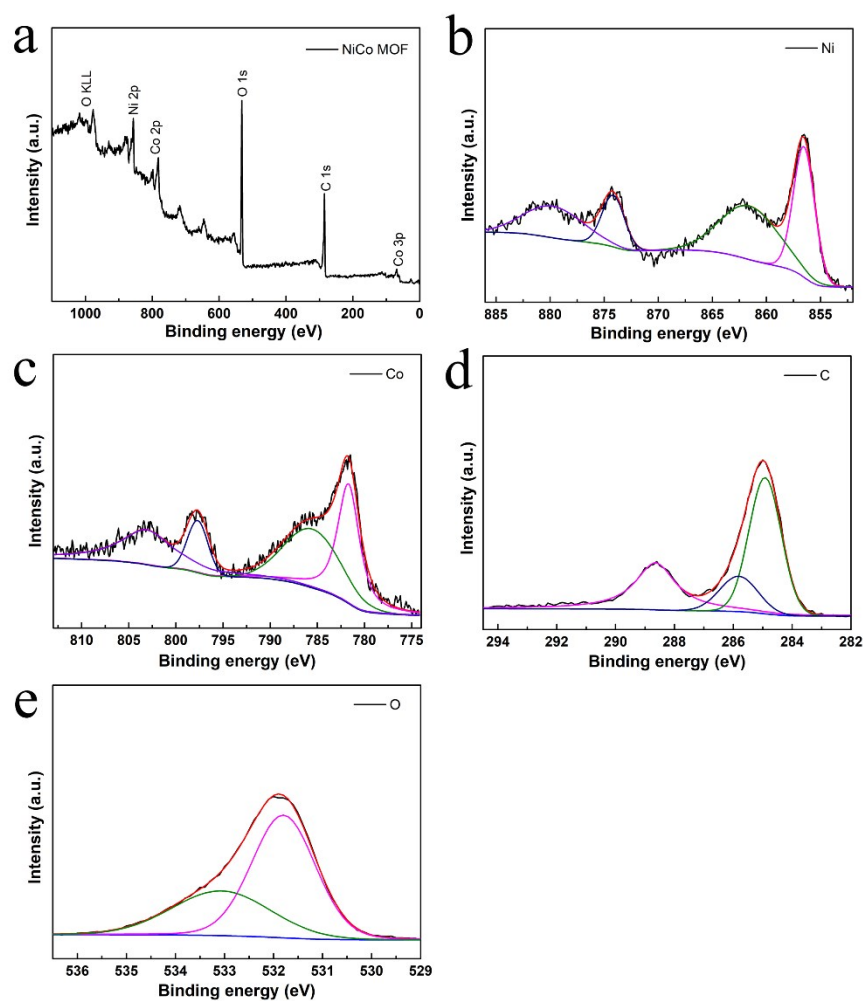
Figure S4. XPS spectra of the 2D NiCo MOF sample: (a) survey, (b) Ni 2p, (c) Co 2p, (d) C 1s, and (e) O 1s.
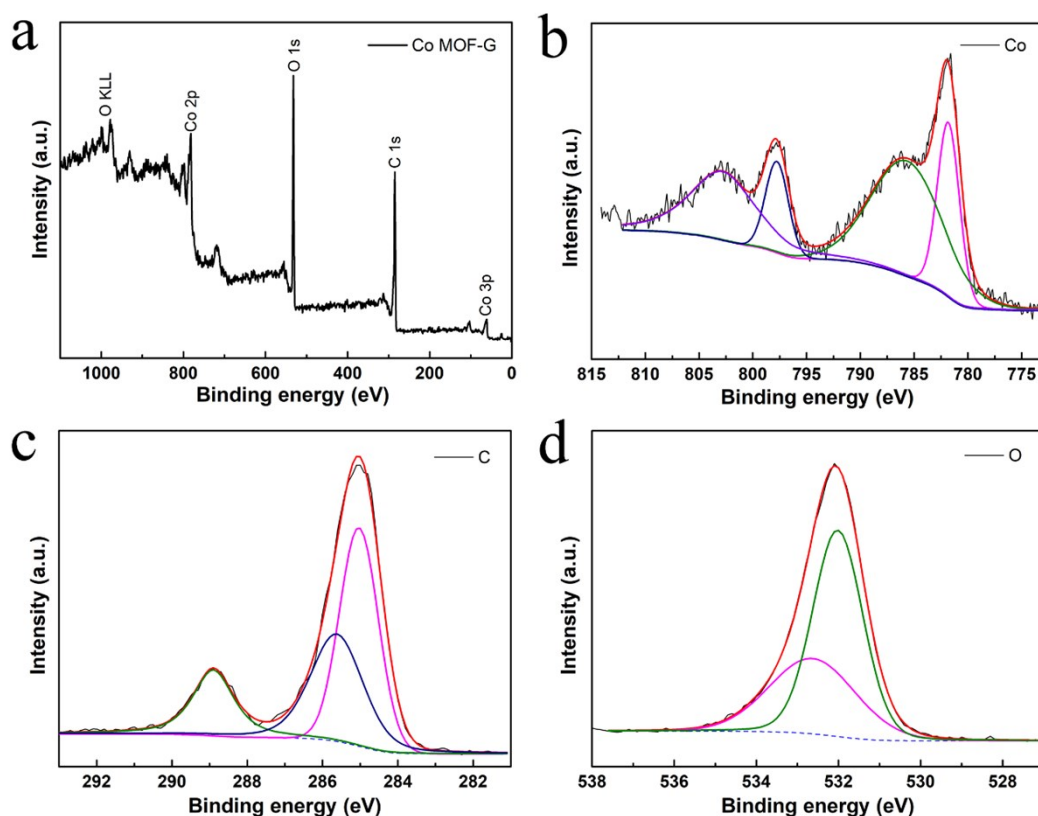
The XPS spectrum in **Figure S4a** confirms the existence of Ni, Co, C, and O elements in NiCo MOF. The two peaks at 856.5 and 874.2 eV in the Ni 2p spectrum (**Figure S4b**) are assigned to Ni $2p_{3/2}$ and Ni $2p_{1/2}$, respectively. The two peaks at 781.7 and 797.7 eV in the Co 2p spectrum (**Figure S4c**) are ascribed to Co $2p_{3/2}$ and Co $2p_{1/2}$, respectively. In the C spectrum (**Figure S4d**), three fitted peaks at 284.9, 285.8, and 288.6 eV are attributed to C=C, C–C and O=C–O, respectively. The O spectrum (**Figure S4e**) shows two fitted peaks at 531.8 and 533.0 eV, which are ascribed to the hydroxyl and chemisorbed water, respectively.
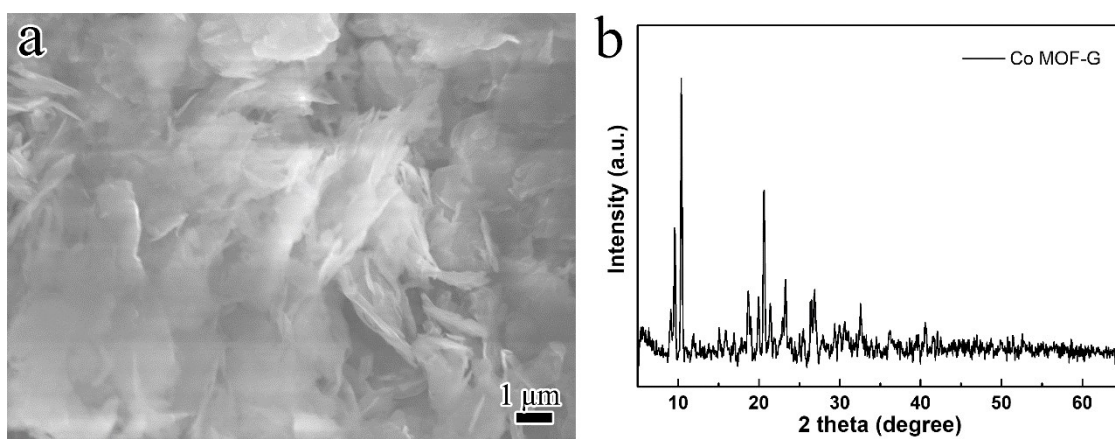
**Figure S5.** (a) SEM image and (b) XRD pattern of the 2D Co MOF-G hybrid.
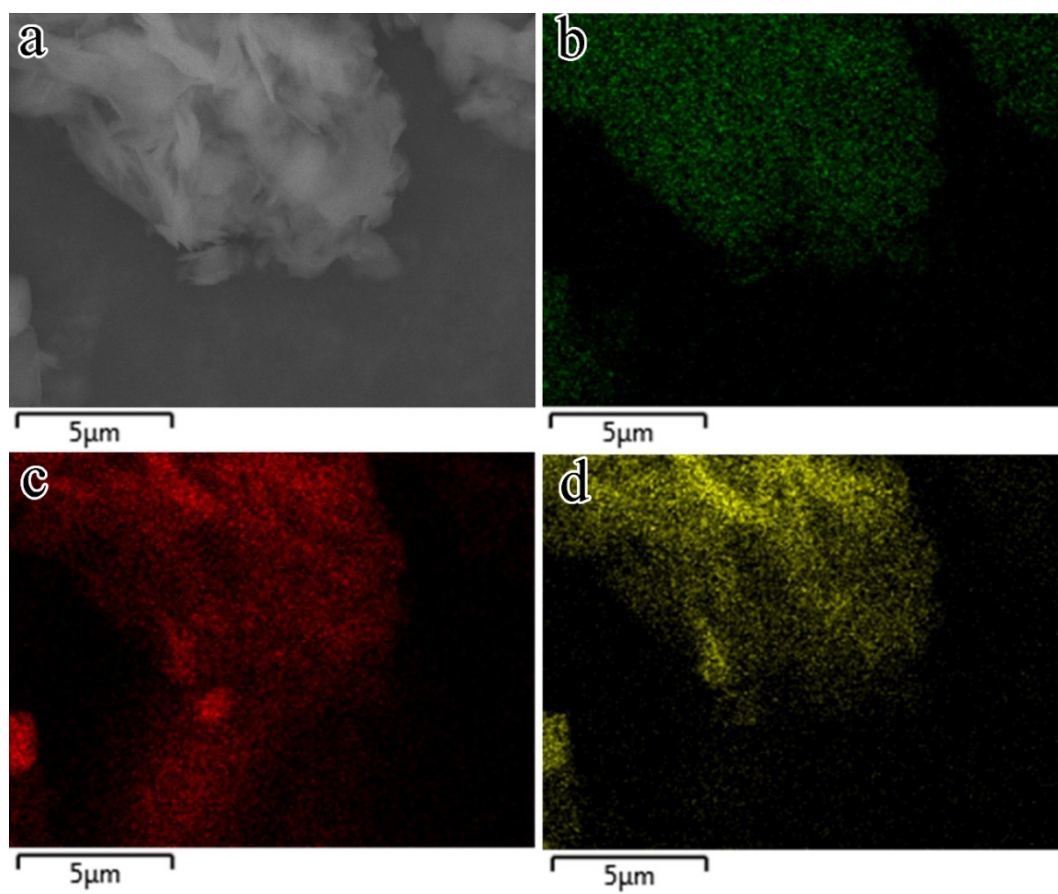
Figure S6. SEM-EDS mapping images of the 2D Co MOF-G hybrid: (a) SEM, (b) Co, (c) C, and (d) O elements.

Figure S7. XPS spectra of the 2D Co MOF-G hybrid: (a) survey, (b) Co 2p, (c) C 1s, and (d) O 1s.

The XPS confirms the presence of Co, C, and O elements in the Co MOF-G hybrid **(Figure S7a)**. The Co 2p spectrum (**Figure S7b**) demonstrates two main peaks at 781.9 and 797.8 eV assigned to Co $2p_{3/2}$ and Co $2p_{1/2}$, together with two corresponding satellite peaks at 786.0 and 803.1 eV, respectively. The C spectrum (**Figure S7c**) depicts three peaks at 285.0, 288.9, and 290.0 eV, which are assigned to C=C, C–C and O=C–O, respectively. The O spectrum (**Figure S7d**) possesses two peaks at 531.9 and 532.7 eV, which are ascribed to the hydroxyl and chemisorbed water, respectively.
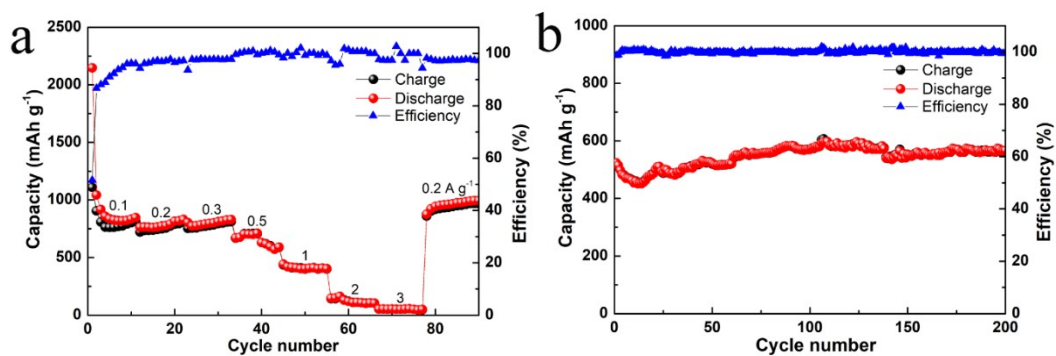
Figure S8. Electrochemical performances of the 2D NiCo MOF electrode: (a) rate performance at different current densities of 0.1, 0.2, 0.3, 0.5, 1, 2, and 3 A g^{-1} and (b) cycle performance at 0.5 A g^{-1}.
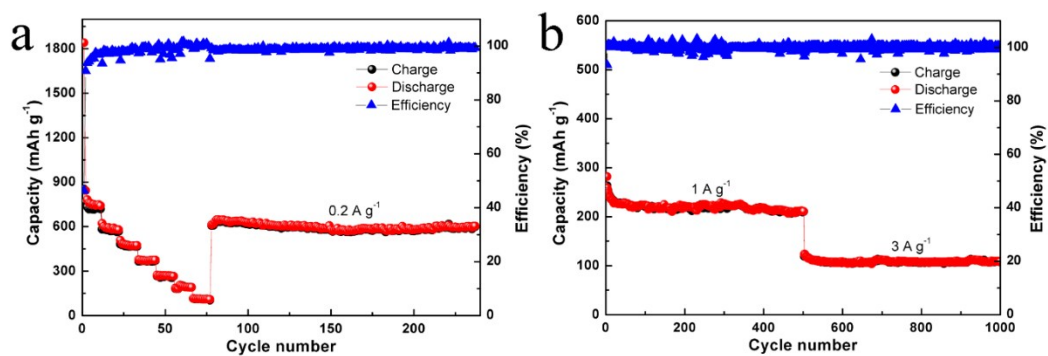
Figure S9. Electrochemical performances of the 2D Co MOF-G electrode: (a) rate performance at different current densities of 0.1, 0.2, 0.3, 0.5, 1, 2, and 3 A g^{-1} and cycle performance at 0.2 A g^{-1} and (b) cycle performance at 1 and 3 A g^{-1}.
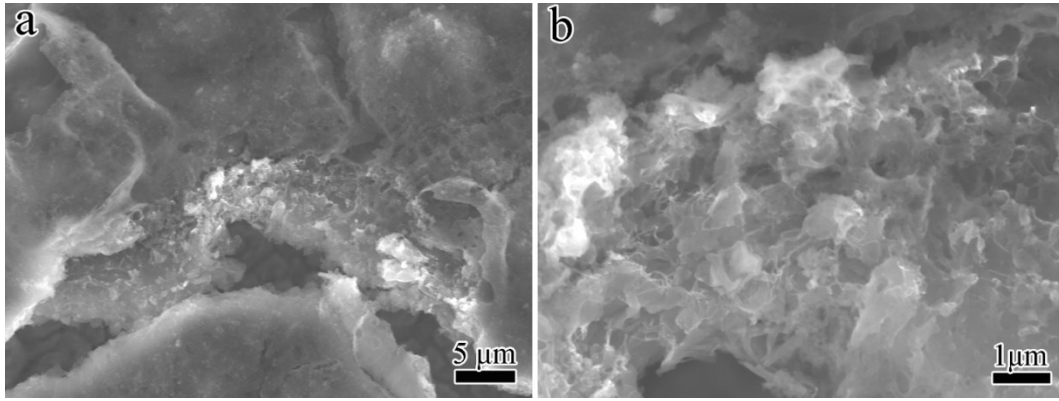
Figure S10. (a, b) SEM images of the hierarchical 2D NiCo MOF-G electrode on the state of discharge after 100 cycles.
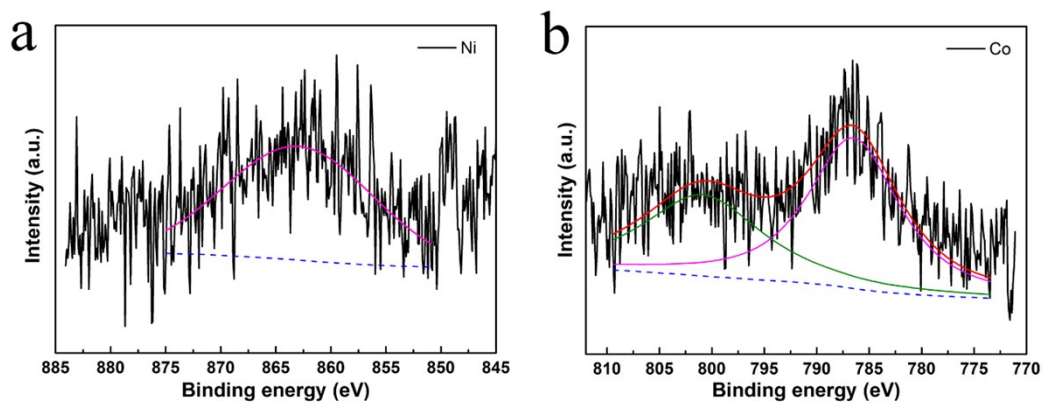
Figure S11. XPS spectra of the 2D NiCo MOF-G electrode after discharge: (a) Ni 2p and (b) Co 2p.

Reference

1. H. Song, L. Shen, J. Wang and C. Wang, Phase segregation and self-nano-crystallization induced high performance Li-storage in metal-organic framework bulks for advanced lithium ion batteries, *Nano Energy*, 2017, **34**, 47-57.

2. Q. Liu, L. Yu, Y. Wang, Y. Ji, J. Horvat, M.-L. Cheng, X. Jia and G. Wang, Manganese-based layered coordination polymer: synthesis, structural characterization, magnetic property, and electrochemical performance in lithium-ion batteries, *Inorg. Chem.*, 2013, **52**, 2817-2822.

3. S. Maiti, A. Pramanik, U. Manju and S. Mahanty, Cu_3(1, 3, 5-benzenetricarboxylate)$_2$ metal-organic framework: a promising anode material for lithium-ion battery, *Micropor. Mesopor. Mater.*, 2016, **226**, 353-359.

4. S. He, X. Zhou, Z. Li, J. Wang, L. Ma and S. Yang, Fluorine doping strengthens the lithium-storage properties of the Mn-based metal-organic framework, *ACS Appl. Mater. Interfaces*, 2017, **9**, 26907-26914.

5. Y. Wang, Q. Qu, G. Liu, V. S. Battaglia and H. Zheng, Aluminum fumarate-based metal organic frameworks with tremella-like structure as ultrafast and stable anode for lithium-ion batteries, *Nano Energy*, 2017, **39**, 200-210.

6. C. H. Zhang, W. Q. Hu, H. Jiang, J. K. Chang, M. S. Zheng, Q. H. Wu and Q. F. Dong, Electrochemical performance of MIL-53(Fe)@RGO as an organic anode material for Li-ion batteries, *Electrochim. Acta*, 2017, **246**, 528-535.

7. C. Dong and L. Xu, Cobalt-and cadmium-based metal-organic frameworks as high-performance anodes for sodium ion batteries and lithium ion batteries, *ACS Appl. Mater. Interfaces*, 2017, **9**, 7160-7168.

8. Y.-Y. Wang, M. Zhang, S.-L. Li, S.-R. Zhang, W. Xie, J.-S. Qin, Z.-M. Su and Y.-Q. Lan, Diamondoid-structured polymolybdate-based metal-organic frameworks as high-capacity anodes for lithium-ion batteries, *Chem. Commun.*, 2017, **53**, 5204-5207.

9. T. Gong, X. Lou, E.-Q. Gao and B. Hu, Pillared-layer metal-organic frameworks for improved lithium-ion storage performance, *ACS Appl. Mater. Interfaces*, 2017, **9**, 21839-21847.

10. C. Li, X. Hu, X. Lou, L. Zhang, Y. Wang, J.-P. Amoureux, M. Shen, Q. Chen and B. Hu, The organic-moiety-dominated Li^+ intercalation/deintercalation mechanism of a cobalt-based metal-organic framework, *J. Mater. Chem. A*, 2016, **4**, 16245-16251.

11. X.-M. Lin, J.-L. Niu, J. Lin, L.-M. Wei, L. Hu, G. Zhang and Y.-P. Cai, Lithium-ion-battery anode materials with improved capacity from a metal-organic framework, *Inorg. Chem.*, 2016, **55**, 8244-8247.

12. J. Montero, D. Arenas-Esteban, D. Ávila-Brande, E. Castillo-Martínez, S. Licoccia and J. Carretero-González, Lithium ion storage in 1D and 2D redox active metal-organic frameworks, *Electrochim. Acta*, 2020, **341**, 136063.